Experimental investigations into the effect of at-sea conditions on ship airwake characteristics

Wall, Alanna; Thornhill, Eric; Barber, Hali; McTavish, Sean; Lee, Richard

Publisher's version / Version de l'éditeur:
https://doi.org/10.1016/j.jweia.2022.104933
Journal of Wind Engineering and Industrial Aerodynamics, 223, C, 2022-03-07

Journal of Wind Engineering & Industrial Aerodynamics 223 (2022) 104933

Contents lists available at ScienceDirect

Journal of Wind Engineering & Industrial Aerodynamics

journal homepage: www.elsevier.com/locate/jweia

Experimental investigations into the effect of at-sea conditions on ship airwake characteristics

Alanna Wall [a,*], Eric Thornhill [b], Hali Barber [a], Sean McTavish [a], Richard Lee [a]

[a] National Research Council Canada
[b] Defence Research and Development Canada

ARTICLE INFO

Keywords:
Ship airwake
Shipboard launch and recovery operations
Shipboard helicopter
Wind tunnel
Ship motion
Sea trial

ABSTRACT

Shipboard helicopter operations are significantly impacted by the characteristics of the ship airwake which depend on environmental conditions in addition to the ship superstructure. In this paper, the effect of free stream turbulence, wind speed and ship motion on the airwake frequency spectra of two 1:50 scaled ships with stern flight-decks was investigated using wind tunnel testing. Results from a full-scale sea trial are also presented. Using both the wind tunnel and the sea trial data in ship motion conditions corresponding to medium sea states, results showed the ship motion energy was transmitted to the ship airwake at the motion frequencies. For single-frequency ship motions, the energy transfer occurred at the motion frequency only, whereas for more realistic at-sea ship motions with a range of frequency components the energy was transferred at a broadband of frequencies corresponding to the motion frequency range. The way in which realistic motion component effects combine at sea and the amount of energy added to the airwake in realistic conditions is presented. The impact of incoming atmospheric turbulence was also examined.

1. Introduction

A ship airwake is a highly complex flow field that continually shifts in time and space due to atmospheric winds flowing over the large blunt shape of the superstructure geometry and the motion of the ship. For ships with stern flight-decks, operating a helicopter within the airwake is challenging and affected by many factors as shown in Fig. 1. As indicated in green, aerodynamics relate in some way to most of these factors. The specific characteristics of the atmospheric wind profile, including speed and direction, combine with the ship course and speed to give the relative wind conditions that interact with the superstructure to create the airwake, which affects the aircraft, pilot, and ultimately the safe operating limits. The impact of airwake on helicopter operations has been the subject of study by many nations in the past three decades (Polsky, 2003; Bradley, 2004; AVT-148 Task Group, 2011; Kaaria et al., 2013; Shipman et al., 2008; Rhoades and Healey, 1992; Shukla et al., 2019).

The National Research Council (NRC) has been investigating the flow field of ship airwakes and their impact on unsteady helicopter rotor loads and helicopter operations for over a decade. Wind tunnel testing of model-scale ships is used to support the development of Ship–Helicopter Operational Limits (SHOL), which is the mapping of safe operating envelopes for each combination of ship and helicopter with respect to a relative wind speed and direction (Healey, 1992; Lee and Zan, 2005b,a; Yuan et al., 2018; Zan, 2001; McTavish et al., 2015; Harrison et al., 2019).

Many aspects of the components in Fig. 1 are still being investigated by researchers. The effect of ship motion, defined by the hull design, loading conditions and the seaway, on airwake and operational limits is a major focus of current work internationally (Owen et al., 2020). Over the open ocean where ship–helicopter operations take place, global winds excite the air–sea interface and develop wind-waves and atmospheric turbulence intensity levels that are not present during calm-sea conditions. These additional complexities occurring alongside flow fluctuations resulting from the ship superstructure may make flight-deck operations more difficult.

The images in Fig. 2 show the dynamic working environment for landing a maritime helicopter on the stern flight-deck of a ship for a low sea state (left) and a high sea state (right).

To understand further the complex flow features that contribute to the environment that the maritime helicopter experiences, experimental work has been carried out to investigate the effects of turbulence and ship motion on the flow structures in the ship airwake. Specifically, two model ships with stern flight-decks have been tested in a wind tunnel in conditions which included representative at-sea wind and ship

* Corresponding author.
E-mail address: alanna.wall@nrc-cnrc.gc.ca (A. Wall).

https://doi.org/10.1016/j.jweia.2022.104933
Received 26 June 2021; Received in revised form 11 February 2022; Accepted 11 February 2022
Available online 7 March 2022

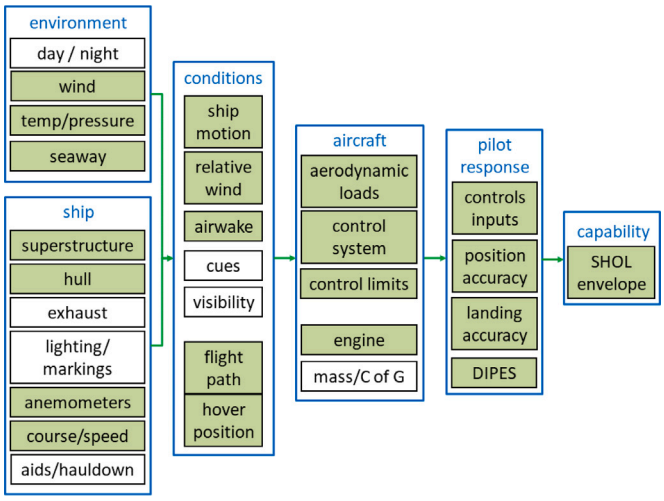

Fig. 1. Factors affecting shipboard helicopter operational limits. Green/shaded identifies those factors influenced by aerodynamics.

motion conditions. Results from a sea trial are used to compare with the wind tunnel results and develop final conclusions.

2. Background

During shipboard operations, the combination of prevailing winds and the forward motion of the ship results in a relative wind that flows over and around the ship. Due to the wide variation in possibilities for a ship geometry, each ship has a unique airwake. The flow separates at the sharp corners of the aft face of the hangar forming a shear layer between the fast moving freestream flow and a recirculation zone, behind the hangar. As some flow is drawn into the low pressure recirculation zone, a circulation pattern creates fluctuating structures which are released as pressure builds. Additionally, flow from the hull sides climbs over the deck edge and joins the recirculation zone, moving towards and up the hangar face (Healey, 1992). The complex integration of these airwake features is also influenced by the apparent yaw of on-coming winds that introduce angularity to the flow field.

The development of the flow field around ships at sea occurs in the presence of the atmospheric winds and pre-existing turbulence in the atmosphere. For a simulation to represent a typical at-sea condition, turbulence intensity is considered critical (Healey, 1992; Polsky, 2003; Rahimpour and Oshkai, 2016). Healey (Healey, 1992) recommends a turbulence intensity between 13% and 17% for atmospheric turbulence over rough seas at a reference height of 10 m above sea level (ASL). This range is in agreement with observations on high-wind turbulent structures above open seas where measurements were taken at 8 m ASL from a buoy placed 5 km offshore (SethuRaman, 1979). For wind speeds above 12 m/s, the standard deviation (σ_u) in streamwise flow is reported by SethuRaman (SethuRaman, 1979) to follow a linear trend of $\sigma_u = 0.2u$ - 1.06, translating into a turbulence intensity of:

$$I_u = 0.2 - 1.06/u \tag{1}$$

where u is the atmospheric wind speed in m/s.

For at-sea wind speeds between 12 m/s and 30 m/s this relation predicts a turbulence intensity of between 11% and 16% at a height similar to a typical flight-deck, when referenced to the mean wind speed at that location. Relative wind speeds that result from the combination of atmospheric winds and ship forward speed are subject to a decrease in apparent turbulence intensity compared to the level in the atmosphere as observed from the perspective of the ship.

From wind tunnel testing of a scale model of a Canadian Coast Guard icebreaker, particle image velocimetry (PIV) results showed that the addition of atmospheric boundary layer (ABL) turbulence changed the number and size of the recirculation zones, and the locations of maximum turbulence within the ship airwake (Rahimpour and Oshkai, 2016). The change in patterns of recirculation may result from shear layer distortion caused by the presence of turbulence. From a study on the flow around rectangular-shaped bodies, it was found that free-stream turbulence intensity increases the curvature of the bluff-body shear layers, shortening the reattachment distance (Meroney, 1988; Polsky, 2003).

Two recent studies found that ABL turbulence resulted in an increase in turbulence over the flight deck. The first used the Office of Naval Research (ONR) Tumblehome ship geometry (Dooley et al., 2019; Krebill, 2020), and the second used the Simple Frigate Shape 2 (SFS2) (Thedin et al., 2019). In contrast also using the SFS2, a different research group observed a slight decrease in deck turbulence intensities with the ABL (Seth et al., 2020). They also observed a more diffuse shear layer in the airwake with ABL turbulence which is consistent with the findings of the other studies. Insufficient experimental details are given to allow speculation as to the cause of their differing result, however a different definition of "turbulence intensity", for example normalizing by the local flow speed, could lead to this seemingly contrasting conclusion.

These works have studied the effects of turbulence on the wake of a stationary ship in the absence of the low-frequency fluctuations in wind speed and direction that are present in the atmosphere. Ship motions further complicate airflow features. In 2017, a PIV study of the SFS2 undergoing pitch motion was published (Sydney et al., 2017). This study revealed three important conclusions about the effect of ship motion on airwake that are consistent with early work on ship motion effects (Owen et al., 2020):

- ship motion induces additional unsteadiness into a ship airwake;
- the additional unsteadiness occurs at the motion frequency; and
- there is a phase lag associated with the airwake response compared to the ship motion.

A computational fluid dynamics (CFD) and PIV study conducted using the ONR Tumblehome ship geometry undergoing pitch and heave motions identified similar observations as those indicated above (Dooley et al., 2019, 2020; Krebill, 2020). Additionally, the study identified new observations, which include the hypothesis that sea states of approximately sea state 3 or less do not significantly affect the ship airwake. This corroborates previous unpublished observations by NRC; however it is likely this observation is valid not as a function of the sea state only, but rather for the relative amount of ship motion in sea state 3 compared to the size of the ship. Larger ships or ships with active stabilization may be able to sustain higher sea states without significant airwake effects at higher sea states.

It has been long recognized that airwake unsteadiness impacts pilot response, where some frequencies are more problematic than others (McRuer, 1994). Frequencies at the low end of the spectrum are widely accepted to add most significantly to pilot workload, which influences the safe operating envelope. Historically, a frequency range of 0.2 Hz to 2.0 Hz has been used for ship–helicopter studies; however, as the body of work expands to include new low-frequency phenomena, the low-end of this range needs to be reconsidered (Harrison et al., 2019). In general, large amplitude fluctuations in the key frequency range add to pilot workload. Flight simulations indicate that an oscillating behaviour of the ship airwake at certain frequencies may increase the challenge associated with operating in the airwake (Shi et al., 2019); therefore, correct simulation of airwake features is important to assess the impacts on operations. Oscillating frequencies can come from the atmosphere and from the oscillating motion of the ship. Periodic oscillations manifest in the flow spectra as frequency peaks. For the ship airwake, the largest atmospheric fluctuations and ship motion frequencies are typically present at the low end of the spectrum (< 2.0 Hz).

Fig. 2. Ship–helicopter operations on a stern flight-deck. Left side: low sea state (Skies Magazine, 2019), right side: high sea state (Society of Rock, 2020).

Table 1
Ship characteristic dimensions and probe locations. Dimensions are expressed in equivalent full scale meters; models were at 1:50 scale.

Ship Characteristic	GD [m]	CPF [m]
Length overall L_{oa}	150	135
Length superstructure L_s	71	71.5
Length flight deck L_f	29.5	23
Width overall B_{oa}	22	16.5
Width superstructure B_s	19	16
Height high hover HH	9.5	9.5
Height superstructure H_s	8	7

Given that low frequency airwake oscillations have the potential to be significant for helicopter operations and have not yet been widely studied, this paper examines the presence of such peak frequencies in ship airwakes for two model ships as well as a real ship at sea.

3. Experimental details

3.1. Ship models and probe locations

Airwake measurements were taken for two ship types: a Generic Destroyer (GD) and a Canadian Patrol Frigate (CPF). The CPF airwake investigation was part of a series of studies for Canada's Department of National Defence (DND) using modelling and simulation tools to support safe and efficient shipboard helicopter operations. In this paper, two types of measurements are presented: those collected in the wind tunnel (WT), and those collected during a sea trial (ST).

The GD is a notional warship design, created by Defence Research and Development Canada (DRDC) as a test case for the development and testing of modelling and simulation tools. The features of the GD are coarse, with a resolution on the order of 3 m full-scale. The version of the GD tested was the NATO-GD (Owen et al., 2020; Wall et al., 2020b).

The CPF wind tunnel model is based on the Canadian HALIFAX-class frigate, though certain smaller sized features (< 1 m), such as deck railings, were neglected. These smaller features add to modelling complexity and have not been found to play a significant role in airwake characteristics. Equivalent sea trial airwake measurements were taken aboard the HALIFAX-class frigates HMCS MONTREAL and HMCS ST JOHN'S.

The major differences between the GD and the CPF are the details of the superstructure, including the leading face and the presence of gaps between structures for the CPF. The ships have a similar flight-deck/hangar beam and superstructure length-to-width ratio. Fig. 3 illustrates key geometric features such as notional rotor diameter (18 m full scale or 360 mm model scale), and typical hover position. The values for the dimensions in Fig. 3 are given in Table 1.

For the wind tunnel data, fast-response pressure probes (Turbulent Flow Instrumentation Pty Ltd - Cobra probes) were used to measure the airwake flow characteristics (Hooper and Musgrove, 1997). The data measured by the Cobra probes provide time-series of the three components of velocity and static pressure from which mean values and turbulence quantities (standard deviation (STD), correlation, frequency spectra) were calculated. At sea, the same flow information was collected using R.M. Young model 8100 3D ultrasonic anemometers.

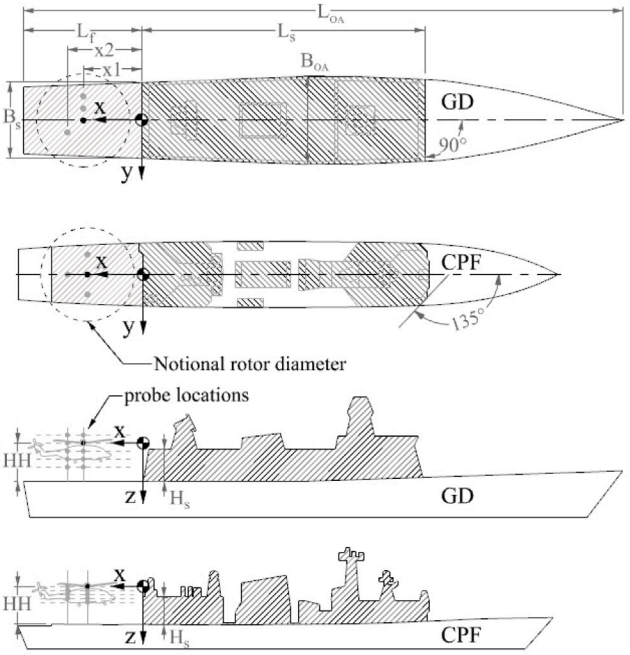

Fig. 3. Generic Destroyer (GD) and Canadian Patrol Frigate (CPF) wind tunnel models schematic.

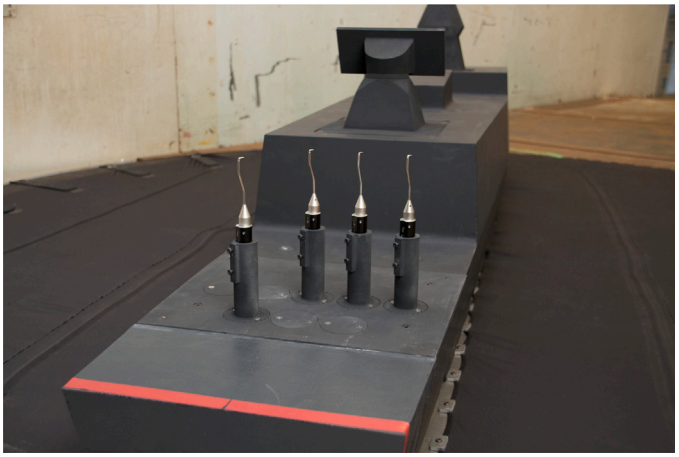

Fig. 4. Cobra probes on GD flight-deck for a G30 relative wind case, where Cobra probes are aligned with freestream wind direction.

On both the CPF and the GD, an array of probes was used and was set to different measurement heights. The CPF, the GD, and the sea trial measurement locations included the same set of probe/anemometer locations, when considered at full-scale. In addition to the standard probe locations, the GD geometry was also used to measure at a greater number of probe locations. For the GD, the four-probe configuration shown in Fig. 4 was mirrored about the centreline to capture either

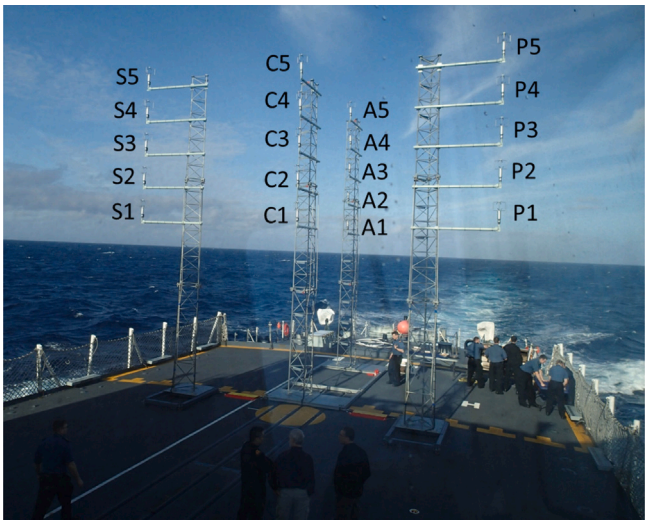

Fig. 5. Flight deck anemometers mounted on HMCS MONTREAL.

Table 2
Locations of selected airwake measurements points at full scale.

Point	x [m]	y [m]	z [m]
S5	14	5	9.5
C5	14	0	9.5
P5	14	−5	9.5
A5	19	0	9.5
S4	14	5	8.5
C4	14	0	8.5
P4	14	−5	8.5
A4	19	0	8.5
S3	14	5	7.5
C3	14	0	7.5
P3	14	−5	7.5
A3	19	0	7.5

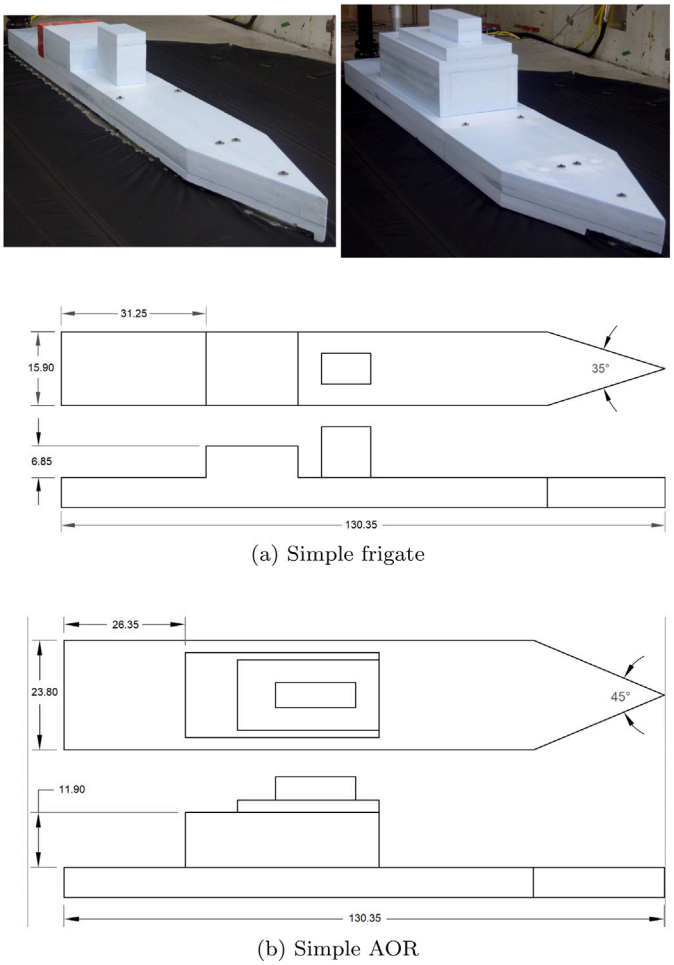

Fig. 6. Simple frigate and AOR models. Dimensions are expressed in equivalent full scale meters; models were at 1:50 scale.

port or starboard flow characteristics. The black marker shown over the flight decks of the CPF and GD models in Fig. 3 illustrates the centre of the nominal high hover rotor disc, point C5, which is the point used for the results presented in this paper. The grey markers illustrate the other measurement locations that are not discussed in this paper.

Fig. 5 shows the ultrasonic anemometers at the measurement points for the ST with the associated nomenclature for each point location (S - Starboard; C - Centre; P - Port; A - Aft). Locations of the measurement points on the CPF are given in Table 2 with respect to the coordinate system shown in Fig. 3. The sonic anemometers used at sea are capable of measurements for the full azimuthal range and pitch up to 60° from horizontal; data were acquired simultaneously from all 20 anemometers throughout the trial.

In the wind tunnel, each probe was mounted in a sleeve allowing rotation and adjustment of height. Although the influence of the probe holders has yet to be fully characterized, validation against sea trial and CFD to date has shown good agreement (Yuan et al., 2018). The authors believe this is because the flow at the measurement height is unaffected by minor disturbances close to the deck. Also, for airwake studies with the GD probes mounted from above at the same measurement locations, poorer agreement was found with the sea trial and CFD data due to the probe rig influence. Therefore, the results for a configuration with the deck-mounted probes is considered more accurate.

Measurements were taken at five heights referenced to the typical helicopter high hover, which has the centre of the nominal rotor disc at 9.5 m (190 mm model scale) above deck. The GD and CPF probe heights were incremented by 2 m and 1 m full scale, respectively. In the wind tunnel, the ships were oriented for 0°, 15° and 30° relative wind conditions. The CPF was tested in relative winds from both directions, while the GD was tested only for winds from starboard. For all configurations, including yaw, the probes were oriented along the wind tunnel axis, to maximize in-range data for the ±45° acceptance cone of the probe. This approach maximized the un-clipped data over the full data set, without the need to tune the probe angles for each position. Due to the extremely turbulent nature of ship airwake flow, some data are out of range of the Cobra probe measurement cone for specific yaw angles. The effects of this "clipping" on Cobra probe measurements are discussed in detail elsewhere (Wall et al., 2020a); these effects are not present in the data used for this paper.

The effect of ship geometry on response to ship motion was examined during a different measurement campaign using the Helicopter Unsteady Loads Measurement System (HULMS) (McTavish et al., 2015), which is a scaled rotor system immersed in the ship airwake. The HULMS is primarily used to measure the unsteady rotor thrust, $Fzrotor$, on a helicopter model, which is an indicator of the unsteadiness and associated pilot workload over the flight deck. In addition to immersion of the scaled rotor into the wake of the CPF, the wakes of a simplified frigate and a simplified Auxiliary Oil Replenishment (AOR) shape were also studied. Fig. 6 shows the geometry of these models.

3.2. Wind tunnel experiments

The WT experimental work was carried out at the NRC 3 m × 6 m Wind Tunnel. The tunnel is an open-circuit wind tunnel with a 3.1 m wide × 5.4 m high × 6.4 m long test section. The test setup included

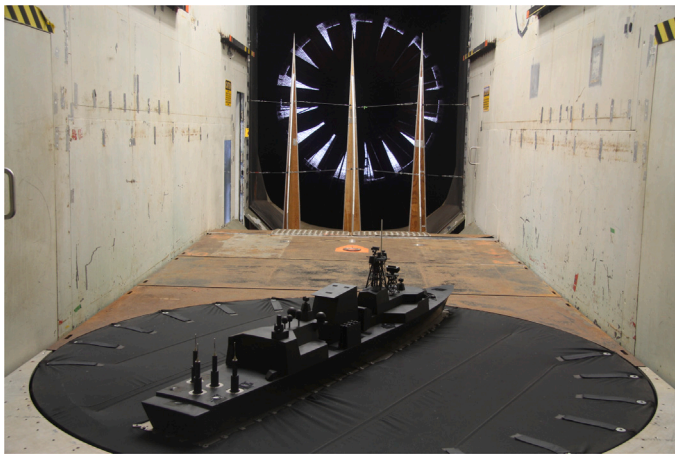

Fig. 7. 1:50 scaled ship setup in the 3 m × 6 m Wind Tunnel with turbulence spires and fan visible upstream.

flow conditioning and ship-motion to simulate real-world atmospheric, at-sea conditions. Fig. 7 shows the 1:50 scale model of the CPF installed in the test section.

To match the wind tunnel velocity profile and turbulence levels to the ABL above the open sea, spires were installed at the test section inlet. Three triangular spires 3.05 m tall by 0.29 m in base width were used. The inlet flow conditioning was designed to approximate a theoretical ABL velocity profile following the exponential relationship:

$$\frac{U_m}{U_{ref}} = \left(\frac{z}{z_{ref}}\right)^{\alpha} \tag{2}$$

where U_m is the measured wind speed at a distance z above the test section floor which represents the air–sea interface of the open ocean. The fixed reference height, z_{ref} and power-law exponent, α, are defined by North Atlantic Treaty Organization (NATO) as 19.5 m and 0.14 respectively (NATO, 1993). U_{ref} is the reference test section wind speed at height z_{ref}.

Fig. 8 shows the velocity and turbulence profiles at the model location, for several projects at this facility. The ship-model helicopter hover heights for the current test campaign are denoted by the horizontal dashed lines in each plot to clarify that the tunnel turbulence intensity at the model location and within the model height is increased by up to 11% with spire flow conditioning, when referenced to the freestream mean wind speed. Measurements over the years show lateral uniformity across the test section for both smooth and turbulent flow configurations, within the measurement uncertainty which is on the order of 3%. For the 2019 data shown in Fig. 8, points have been added from related flow measurements without spires, referred to as a configuration with smooth flow. The smooth flow data points provide context for results to be discussed, which will demonstrate the impact of ABL turbulence on the ship airwake. The wind tunnel boundary layer is considered a representation of a single real-world ABL that exists within a range of wind profiles that develop over varying sea roughness and for a range in ship speeds.

In comparison with the ST data, the turbulence intensity at sea as measured by the ship anemometers corrected for ship-induced biases (Thornhill et al., 2020) was between 2% and 8%, depending on the flow conditions and the ship speed. In this work, the biases that have been corrected result from flow distortions due to the ship superstructure for a ship in the nominal position without induced ship motion. The reading were not corrected for the influence of ship motion.

Fig. 9 shows the spectra of the incoming flow at the reference height in flow speed, pitch, and yaw at equivalent full scale. Flow speed, pitch,

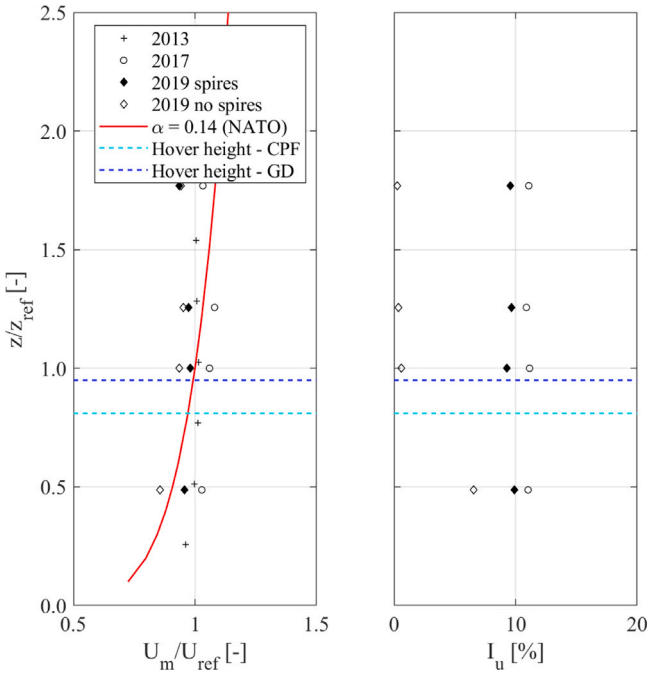

Fig. 8. Wind tunnel flow speed and turbulence profiles at model location measured in the 3 m × 6 m Wind Tunnel. Hover heights correspond to the nominal rotor plane.

and yaw are the outputs of the Cobra probes used to characterize the simulated ABL which describe the three-dimensional flow at each measurement location. The turbulence induced by the spires is relatively broadband, with the exception of flow yaw, where a lateral vortex shedding peak induced by the spires can be seen. It is assumed that the lateral vortex shedding peak is observed because the centre of the ship is located 2.6 spire heights downstream of the spire installation location, which is less than the 6 spire heights recommended in the development of ABL flows in wind tunnels (Irwin, 1979). The spire height and longitudinal position was a compromise between the target conditions and the fetch available in the wind tunnel. Since this peak does not exist in flow speed or pitch, it represents a slight lateral shifting of the flow, on the order of 3°. As will be shown, low frequency lateral variation in the incoming flow at sea is a realistic feature.

To acquire the relevant data for model scale ships with wave motion, the parameters for kinetic and dynamic similitude, respectively, are: (i) reduced frequency (f^*) and (ii) Reynolds number (Re). Since a minimum Re of 11×10^3 is widely accepted for ship airwake modelling (Healey, 1992), and the experimental setup exceeded that by an order of magnitude, the reduced frequency becomes the scaling parameter requiring primary consideration. Reduced frequency is a non-dimensional representation of time and is defined as

$$f^* = \frac{f B_s}{U_{ref}} \tag{3}$$

where, in the context of ship-motion simulations, f is the frequency of an imposed time variation, B_s is the beam of the superstructure, and U_{ref} is the relative wind speed. The reduced frequency relationship between model f^*_m and full-scale prototype f^*_p, then becomes

$$\frac{f^*_m}{f^*_p} = \frac{\lambda_f \lambda_D}{\lambda_{U_{ref}}} = 1 \tag{4}$$

Since the geometric scale, λ_D, is fixed at 1:50 (model:full-size) to be compatible with wind tunnel infrastructure re-used from previous test programmes, a frequency scaling, λ_f, of 1:0.04 and a wind speed scale, $\lambda_{U_{ref}}$, of 1:2 were selected as the best compromise between competing constraints for Reynolds number and motion platform performance; the

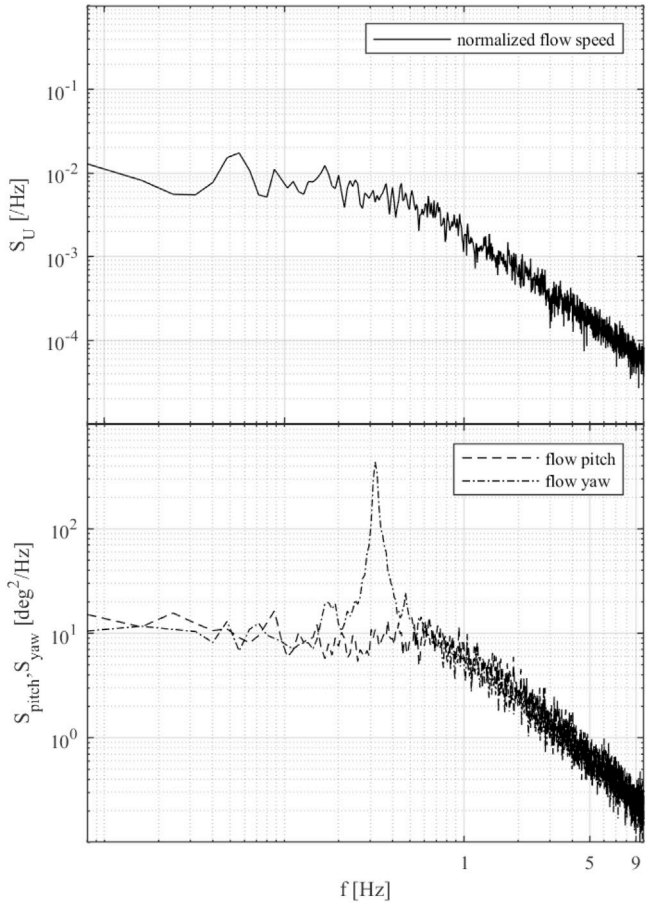

Fig. 9. Spectra of incoming flow with spires at reference height, frequency at equivalent full scale.

motion platform used to generate ship motion in the wind tunnel is described in the next section. The scaled magnitudes of the frequency, wind speed and geometry were used to convert the wind tunnel testing to equivalent full scale values, particularly for comparison with the ST results.

In this paper, dimensional quantities are reported in their equivalent full scale values. Flow speed quantities are normalized with respect to the wind tunnel reference speed, U_{ref}.

3.3. Motion profiles

The ST measurements were conducted in conditions ranging from relatively little ship motion up to moderate ship motions. To simulate ship-motion in the wind tunnel, the test setup includes a NOTUS hexapod, located under the test section and within a turntable structure. At rest, the platform of the hexapod is flush with the test section floor to which the models are mounted, as shown previously in Fig. 7. A fabric skirting is connected to the bottom of the models at the waterline of the ship and the perimeter of the turntable, which represents a mean ocean surface. This allows the motion platform and ship to move freely while prohibiting air flow through the space between the model and static test section floor. The model of the CPF is shown at its maximum roll position in Fig. 10 to illustrate the behaviour of the fabric floor at large-amplitude motions.

When in motion, the platform oscillates according to pre-determined profiles representative of at-sea ship motions. Although the hexapod is capable of 6-degree of freedom motion, only the ship motions of heave, roll, and pitch were simulated. Variations in yaw are examined

Fig. 10. Downstream view of 1:50 scaled ship in maximum roll position in the 3 m × 6 m Wind Tunnel.

statically by varying the relative wind direction for different cases, and surge and sway are not simulated as they are not believed to impact significantly airwake topology. An understanding of the effect of ship motion was accomplished by using motion profiles of increasing complexity.

Sinusoidal motions were used to understand the basic effects of motion resulting from parametric variations in the amplitude and frequency of the motions. Although sinusoidal profiles are not matched to a specific representative seaway, the characteristics were selected to be comparable to similar representative seaways. Sinusoidal profiles are either simple, containing only motion in one degree of freedom, or combined, containing motion for two or all three ship-motion degrees of freedom.

Realistic profiles were created by Defence Research and Development Canada (DRDC) using seaway characteristics specified in Table 4 and the numerical ship motion simulation tool ShipMo3D (McTaggart, 2010). Realistic profiles include heave, roll, and pitch motions phased together. Regular profiles contain only one wave frequency component in the simulated seaway, whereas irregular profiles contain multiple wave frequency components according to a Bretschneider spectrum.

For the irregular profiles, the motion characteristics are representative of the open North Atlantic (NATO, 1993) for Sea State 4 to Sea State 6 shown in Table 3 (NATO, 1993).

Table 4 lists the parameters required to simulate the corresponding motion profile. Fig. 11 shows an example of each type of motion profile, labelled according to the case as defined in Table 4. Motion case 12 shows an example of ship motion in a simulated realistic seaway. In this case, uni-directional waves were modelled, leading to a profile lacking roll. Motion case 13 shows an example of a real ship motion profile measured during the sea trial for headwinds conditions. For this study, relative wind and wave direction were taken to be coincident for the wind tunnel experiments; this condition is common, although not universally the case for realistic conditions at sea.

3.4. Wind definitions

Above the previously-defined minimum Reynolds number of 11×10^3, airwake topology is largely unchanged with wind speed for sharp-edged ship geometries (Healey, 1992). Therefore, a single wind speed was used to characterize the airwake for all of the different wind direction and wave conditions. A model scale wind speed of 10 m/s (19 kts) was selected, which corresponds to a full scale relative wind speed of 20 m/s (39 kts). This wind speed falls in the middle of a typical operational wind speed range for shipboard helicopters.

For the realistic motion profiles for the GD the frequency components were selected to model two full scale ship speeds, 10 kts and

Table 3
Sea state table for the open North Atlantic (adapted from NATO, 1993) (NATO, 1993).

Sea state	Significant wave height (m)		Sustained wind speed (knots)		Modal wave period (s)	
	Range	Mean	Range	Mean	Range	Most probable
0–1	0–0.1	0.05	0–6	3	–	–
2	0.1–0.5	0.3	7–10	8.5	3.3–12.8	7.5
3	0.5–1.25	0.88	11–16	13.5	5.0–14.8	7.5
4	1.25–2.5	1.88	17–21	19	6.1–15.2	8.8
5	2.5–4	5	22–27	24.5	8.3–15.5	9.7
6	4–6	5	28–47	37.5	9.8–16.2	12.4
7	6–9	7.5	48–55	51.5	11.8–18.5	15.0
8	9–14	11.5	56–63	59.5	14.2–18.6	18.64
>8	>14	>14	>63	>63	18.0–23.7	20.0

Table 4
Hexapod motion profile parameters. All quantities given in equivalent full scale values.

#	Type	Ship	Characteristics
0	No-motion	Both	–
1	Simple sinusoidal	GD	heave, A=2.2 m, Mp=25s
2	Simple sinusoidal	GD	roll, A=5°, Mp=25s
3	Simple sinusoidal	GD	pitch, A=5°, Mp=25s
4	Simple sinusoidal	CPF	heave, A=1.5 m, Mp=12.5s
5	Simple sinusoidal	CPF	roll, A=5°, Mp=12.5s
6	Simple sinusoidal	CPF	pitch, A=3.4°, Mp=12.5s
–	Combined sinusoidal	CPF	combinations of 4–6
7	Realistic regular	CPF	Hs=4 m, Tp=15 s, Vs=0 m/s, H=0
8	Realistic regular	CPF	Hs=4 m, Tp=11 s, Vs=0 m/s, H=0
9	Realistic regular	CPF	Hs=2 m, Tp=15 s, Vs=0 m/s, H=0
10	Realistic regular	CPF	Hs=6 m, Tp=15 s, Vs=0 m/s, H=0
11	Realistic regular	CPF	Hs=6 m, Tp=12 s, Vs=0 m/s, H=0
12	Realistic irregular	CPF	Hs=4 m, Tp=15 s, Vs=0 m/s, H=0
13	Realistic irregular	ST JOHN'S	Medium seas, Vs=3.8 m/s, H=0

A	amplitude
Mp	motion period
Hs	significant wave height
Tp	wave period
Vs	ship speed
H	ship heading

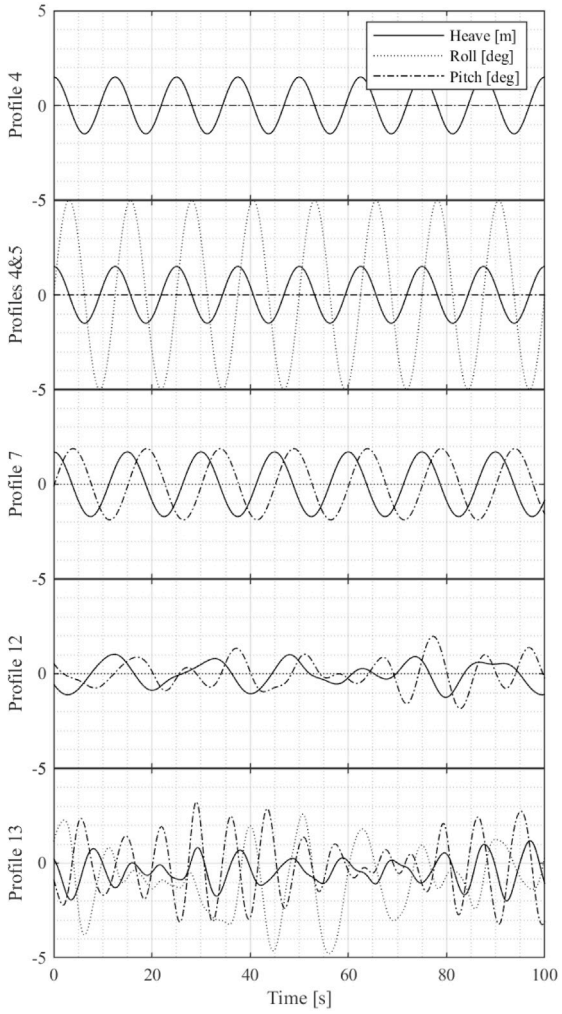

Fig. 11. Sample motion profiles for GD and CPF tests.

15 kts, so that the scope of the tests also included a range of ratios of ship speed to on-coming atmospheric wind.

Wind speed results from WT tests were normalized using the reference speed of the test section as calculated from the tunnel contraction pressure. The wind speeds in this paper are the relative wind speeds, which are the vector sum of the ship speed and the atmospheric wind relative to the centreline of the ship. Except in a few clearly identified cases, results in this paper are for headwind conditions.

The ST relative wind speed and direction is computed from the measurements taken by the ship anemometer system. These measurements are corrected for superstructure-induced biases (Thornhill et al., 2020), but not for the effects of ship motion on the readings.

4. Results

4.1. Validation of wind tunnel data using sea trial data

Using the WT data collected for headwinds for the stationary ship and equivalent ST for cases with low ship motions, the means and standard deviations of the flow speed (U), pitch and yaw at the measurements locations shown in Fig. 5 have been compared in Figs. 12 through 14 for the flow speed, pitch and yaw, respectively. The data points presented are those for which the Cobra probe measurements are not subject to significant clipping due to the 45° acceptance cone. In each image, the measurement points are shown in their relative positions. The left hand side of each circle surrounding the measurement point represents the WT data and the right side, the average ST data. The size of the circle is a measure of the STD according to the inset legend on the right and the colour of the circle is a measure of the mean value, as shown by the contour legend. All three plots illustrate that the trends in the two sets of data are in general agreement.

In general, the WT predicts a higher airwake flow speed than the sea trial. This could be due to uncertainties in the anemometer bias corrections (Thornhill et al., 2020) used to calculate the equivalent relative wind condition or differences in the atmospheric boundary layer over that simulated in the wind tunnel. In general, the agreement in unsteadiness in flow speed between the two data sets is within 5% of the free stream wind speed. The agreement in flow pitch and yaw angle means are almost all within 5° and the standard deviations are generally within 2°. Overall, the wind tunnel simulation closely represents the shape, trends and fluctuations present in the airwake of the ST ship.

4.2. Sensitivity to atmospheric turbulence

The influence of atmospheric turbulence can be shown using two data sets.

First, WT airwake data were collected for the GD with and without spires installed at the inlet of the test section, which allowed a comparison of the effect of atmospheric turbulence. The top image in Fig. 15 shows the normalized flow speed spectra up to 1 Hz for data collected

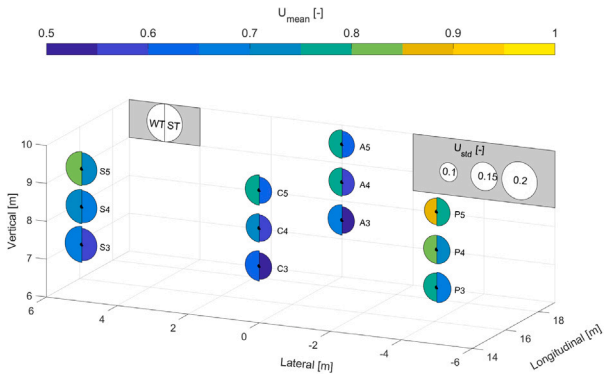

Fig. 12. Comparison of WT and ST flow speed data for headwinds. (For interpretation of the references to colour in this figure legend, the reader is referred to the web version of this article.)

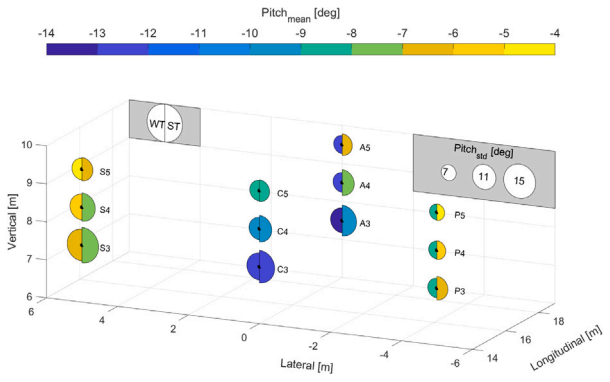

Fig. 13. Comparison of WT and ST flow pitch data for headwinds. (For interpretation of the references to colour in this figure legend, the reader is referred to the web version of this article.)

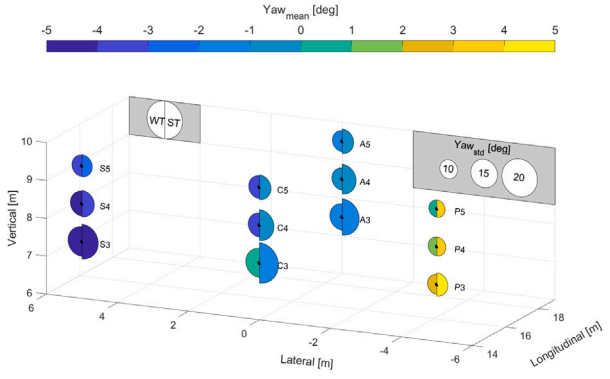

Fig. 14. Comparison of WT and ST flow yaw data for headwinds. (For interpretation of the references to colour in this figure legend, the reader is referred to the web version of this article.)

at hover height (C5). These normalized flow speed spectra at location C5 are compared to spectra from measurements of the incoming flow at the reference height in the absence of a ship. Fig. 15 results are shown for headwind conditions with varying turbulence intensity (I_u), that represent a smooth flow case and an at-sea atmospheric turbulence case, with I_u < 1.0% and I_u = 11%, respectively. Below 0.5 Hz, the airwake turbulence level with the spires is greater than the case without spires, however not to the same degree as the difference in turbulence levels in the incoming flow. This suggests that although flow turbulence is important, the effect is secondary to the turbulence generated by the ship superstructure.

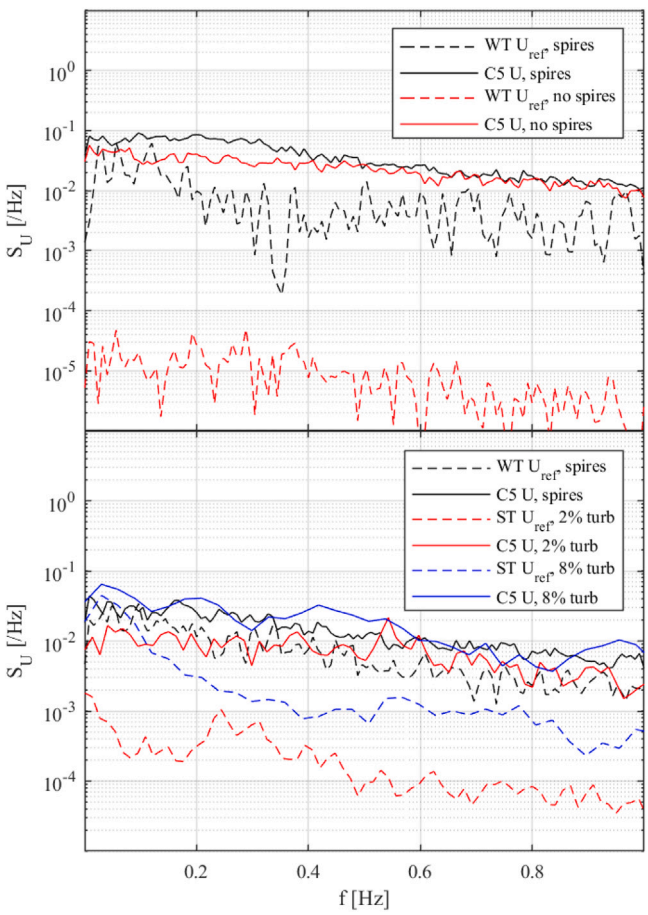

Fig. 15. Variation in flight deck flow for different incoming wind conditions. (For interpretation of the references to colour in this figure legend, the reader is referred to the web version of this article.)

The comparison of CPF data between the WT and ST data sets further corroborates this idea, using measurements in the airwake and measurements of the incident conditions as measured at a reference height by the ship's main anemometers. In the bottom image of Fig. 15, the WT data is compared to two equivalent ST cases, one with a relatively low level of turbulence (2%) and one with a relatively high level (8%). In this case also, increased atmospheric turbulence led to a greater response in the airwake, but to a much lower degree than the variation in the incoming flow. With the exception of the lowest frequencies studied here, which will be discussed later, the airwake spectra measured in all the CPF turbulence conditions could be said to be practically equivalent.

4.3. Effect of motion type

The WT results were used to examine a range of motion types from simple to realistic. From test cases with a range of simple and combined sinusoidal ship motion types, including profiles 4, 5 and 6 from Table 4, CPF data measured at C5 were used to quantify the effects of ship motion on airwake frequency spectra. Fig. 16 shows the results in red and blue in contrast to the no-motion case results shown in black. The top image compares the simple sinusoidal motions, showing that representative pitch and heave give rise to noticeable spectral peaks whereas representative roll has a limited effect.

The second image shows the impact of varying the amplitude and frequency of a simple heave motion profile. The data reveal an intuitive result: higher motion amplitudes correspond to higher amplitudes of induced oscillation in the airwake. Also, higher frequencies of the same

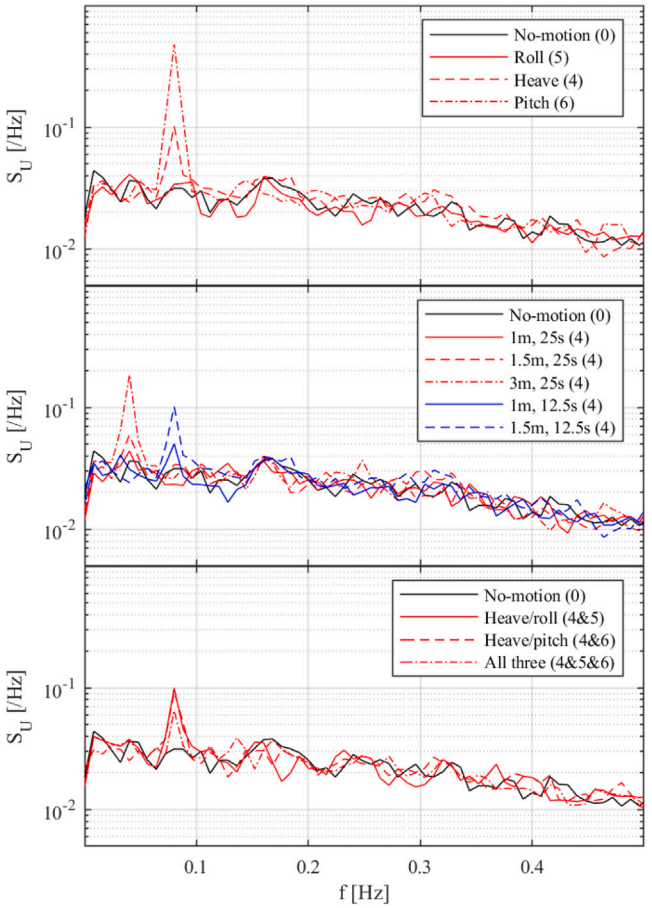

Fig. 16. Influence of sinusoidal ship motions on the spectra of normalized flow speed magnitude. The legends identify the motion direction and, where applicable, the motion parameters. (For interpretation of the references to colour in this figure legend, the reader is referred to the web version of this article.)

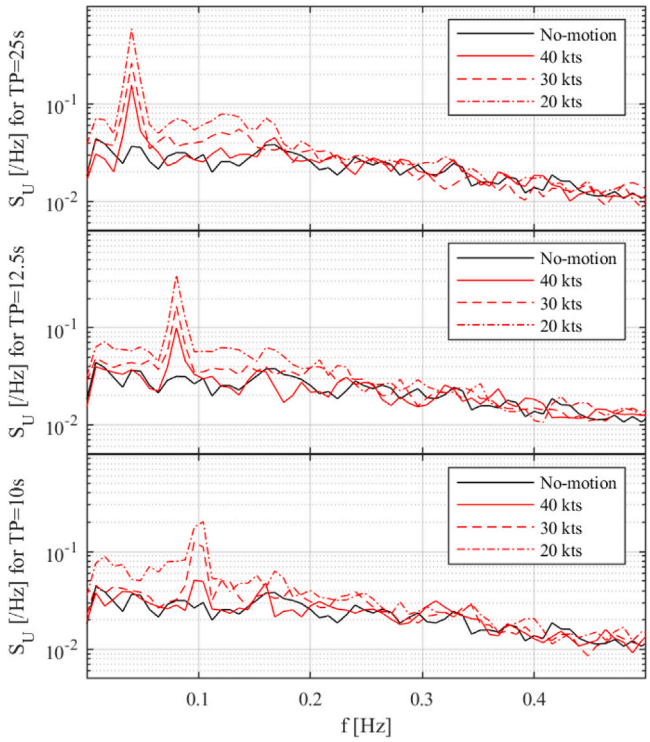

Fig. 17. Influence of wind speed on the motion induced peaks on the spectra of normalized flow speed magnitude. (For interpretation of the references to colour in this figure legend, the reader is referred to the web version of this article.)

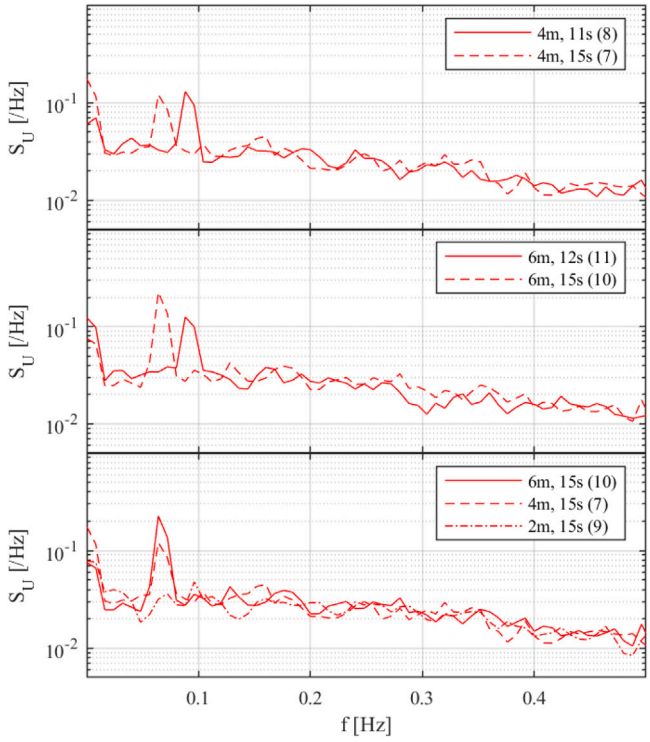

Fig. 18. Influence of significant wave height and wave period for realistic regular ship motion cases.

amplitude of motion induce higher amplitudes of airwake oscillation, although this observation was not a universal result across all cases examined. The combination of two simple sinusoidal motions, as shown in the bottom image, has the effect of decreasing the intensity of the motion-induced flow response for the normalized flow speed.

Fig. 17 illustrates the motion peaks (red) for a motion profile combination (4 & 5) for a range of wind speeds and wave periods. The results are compared to the no-motion case (black) with a wind speed of 40 kts. All results indicate that the transfer of ship motion energy to the airwake at the motion frequency increases as wind speed decreases.

Fig. 18 shows the effects of amplitude (significant wave height) and frequency (wave period) using realistic regular motion profiles, which have a single frequency with all three motion directions correctly phased together. For these cases, no consistent dependence on the response to the frequency is clear, however the relationship where amplitude of response reflects ship motion amplitude holds.

True ship motions are not sinusoidal, therefore the influence of regular and irregular realistic profiles is compared in Fig. 19. The top image shows the spectra of the normalized flow speed magnitude while the bottom image shows the spectra of the heave component of motion. The spectra shown are from the encoders on the motion platform and reflect the actual motion profile as opposed to the desired profile. Mirroring the observations in the bottom image of Fig. 16, the complexity of the motion profile appears to weaken the motion frequency peaks in the normalized flow speed spectra. The wider the bandwidth of motion frequencies, the more the motion energy is absorbed into the overall airwake spectra.

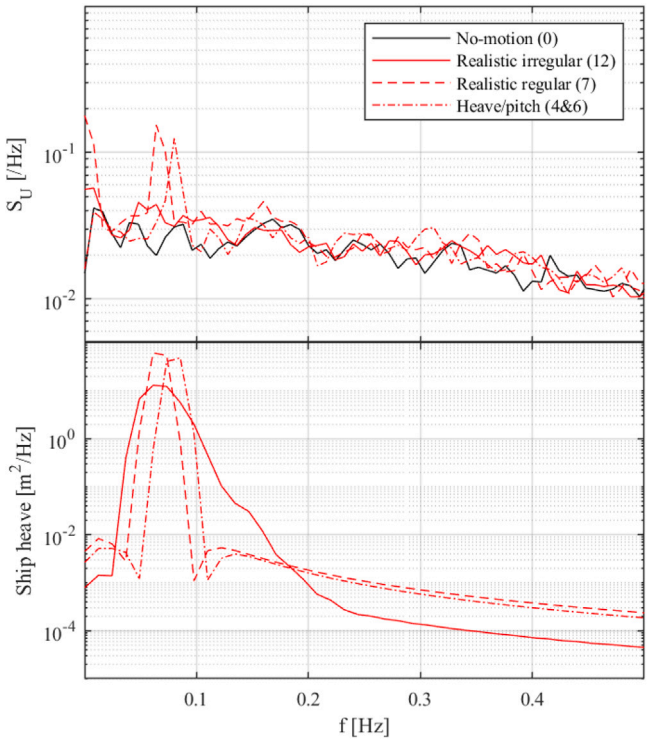

Fig. 19. Influence of motion profile type on the spectra of normalized flow speed magnitude. (For interpretation of the references to colour in this figure legend, the reader is referred to the web version of this article.)

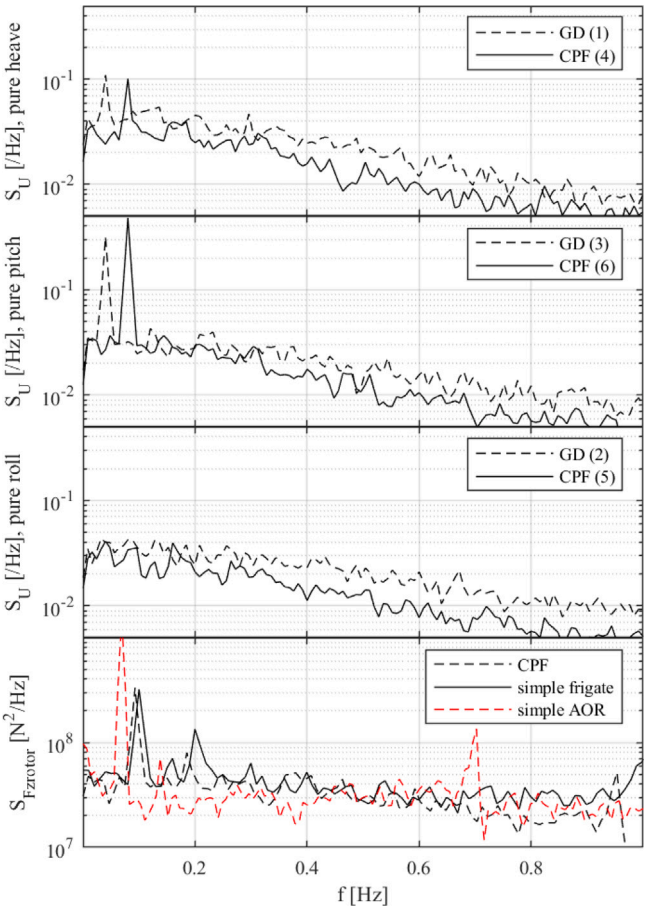

Fig. 20. Impact of geometry on airwake and rotor load spectra. (For interpretation of the references to colour in this figure legend, the reader is referred to the web version of this article.)

4.4. Effect of geometry

The influence of ship geometry can be shown using two data sets. The first data set is based on the airwake measurements of the GD and the CPF. The second data set made use of the two idealized ship models.

Comparing the airwake response of the GD and CPF for similar sinusoidal motions in heave, pitch and roll (top three images respectively in Fig. 20), it can be seen that the response magnitude for both ships is similar.

The HULMS study using the simple models shown in Fig. 6 was also used to examine the effect of geometry on the impact of ship motions. As shown in the bottom image in Fig. 20, the simple AOR leads to a larger amplitude response than the simple frigate. The motion profile for the cases in the bottom image of Fig. 20 was a combined sinusoidal case with a heave amplitude of 1.5 m and a pitch amplitude of 1.7° with a motion period of 12.5 s. This would be expected since the larger superstructure in motion interacts with the flow over more area. This effect occurs in concert with the effect of larger geometry on the no-motion airwake, with larger ships producing larger and slower airwake features (Forrest et al., 2012).

Although the CPF and the simple frigate differ with respect to small geometric details, the motion response is similar owing to their similar size.

4.5. Combination of effects at sea

The wind tunnel results presented thus far have clearly shown the factors that influence the frequency at which motion response occurs and some factors that influence the magnitude. The effect of combining influences has also been examined; however, the ST has revealed key information on the realistic combination of factors in the true at-sea environment. Fig. 21 shows the airwake response at C5 (top image) and the measured ship motion inputs and incoming relative yaw (bottom image) for motion case 13 in Table 4. This case was chosen because the ship pitch and ship roll frequencies are distinct, which clearly shows their independent effects.

The first observation, following on from the earlier discussion about the influence of incoming flow, is that the relative wind yaw contains significant low frequency energy that results in corresponding fluctuations in flow speed and yaw at C5. The incoming relative yaw spectrum also contains energy at the frequency of the ship roll; this is likely due to the fact that the ship anemometers are subject to flow changes induced by their movement with the ship through the incoming flow. Energy at the roll frequency is apparent in the flow yaw at C5; although it is not clearly shown in this data set, flow speed often contains extra energy over the roll frequency range. The ship pitch frequency does not influence the speed and yaw spectra, but clearly impacts the flow pitch at C5, which is sensible considering that pitch occurs on an axis perpendicular to the other parameters.

In general, these data support an intuitive conclusion that the ship airwake responds to fluctuations in the ship and incoming wind at the input frequencies, along the axis where the disturbance exists. In general, these disturbances occur below the traditional lower limit of pilot workload of 0.2 Hz, however the lack of certainty in this lower limit, especially considering that incoming wind and ship motion can impart significant energy at the input frequencies, is worth reviewing. Further, different combinations of parameters such as ship speed or ship size, which increases the encounter frequency of the waves with the ship, may push some of the motion-related airwake energy above 0.2 Hz.

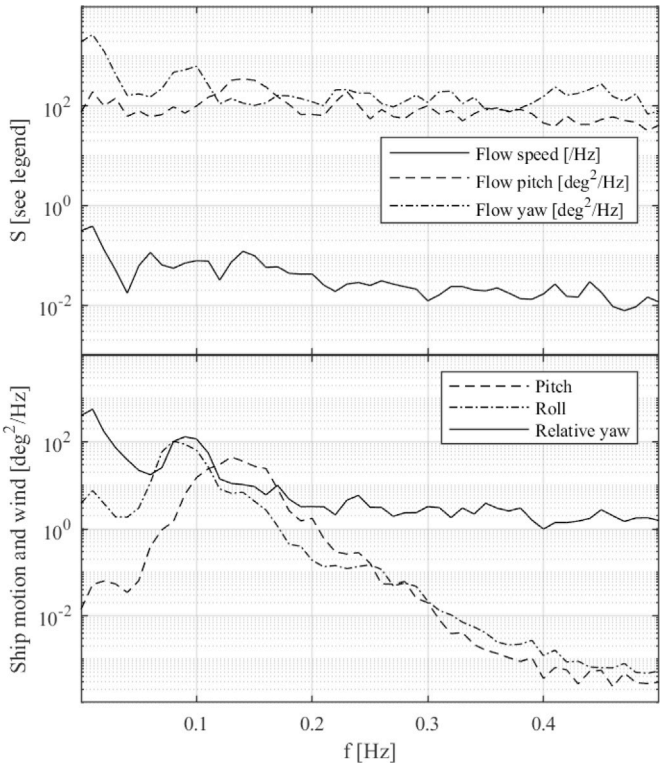

Fig. 21. Influence of motion profile type on the spectra of normalized flow speed magnitude.

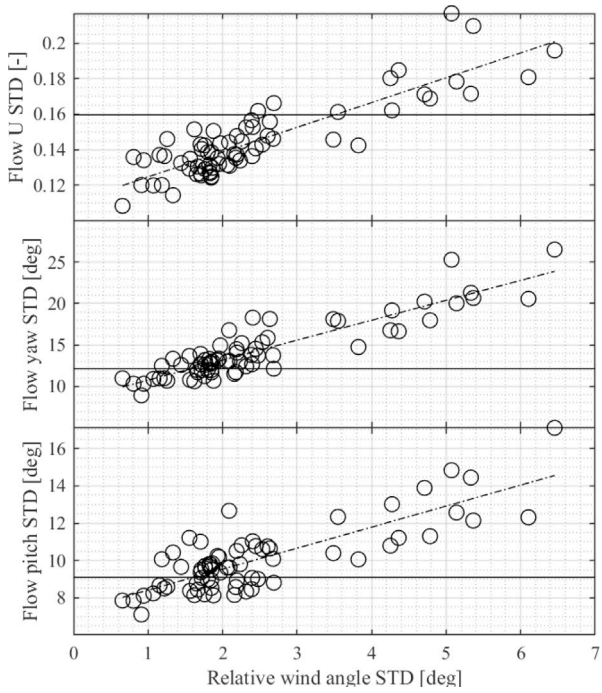

Fig. 22. Relationship between STD of relative wind direction and fluctuations in flow at C5.

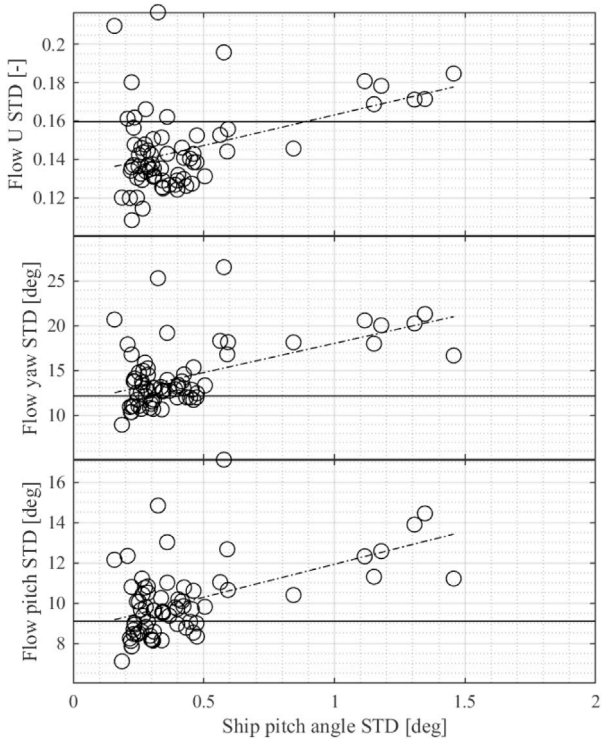

Fig. 23. Relationship between STD of ship pitch and fluctuations in flow at C5.

4.6. Magnitude of motion response at sea

Given the findings described thus far, a remaining question is how to estimate the amount of additional energy that will be added to the airwake for a given ship motion and incoming flow condition. By comparing the standard deviations of the incoming flow and ship motion inputs with the STD of the flow response, some interesting patterns emerge. Shown in Figs. 22 through 24 are these STDs for flow speed, yaw, and pitch compared with relative wind yaw, ship pitch and ship roll, respectively. Shown are all the ST cases for headwinds within 3°, including the 52 low sea state cases summarized previously in Fig. 12 and those for greater ship motions.

In general, the fluctuations in the airwake appear most sensitive to the incoming flow variations and are least sensitive to ship roll. It is interesting that variations in the incoming wind angle alone could possibly be used to predict the variations in the flow due to ship motion; however, this is likely due to the aforementioned fact that the ship anemometer readings are affected by ship motion through their own movement with the ship. This opens up a potential opportunity to use a single parameter as an approximate metric for the amount of additional energy added to the airwake by atmospheric winds and ship motion.

The horizontal lines shown in Figs. 22 through 24 represent the WT values collected for the equivalent condition with no ship motion. In general, the agreement is excellent and the images can be used to infer the approximate ship motion limits that can be considered "low motion". A definition of "low motion" is required to assess which real ship motion cases can be adequately approximated with no-motion data. In the case of ship roll, that limit appears to be around 1.5 or 2°of STD. In the case of ship pitch, the limit appears to be around 0.5° of ship pitch STD for this ship type.

5. Conclusions

The airwake characteristics of two 1:50 ship models were evaluated in smooth and turbulent flow, with and without various ship motion profiles for a range in wind speeds and ship yaw angles. These data have been compared to and analysed in concert with the sea trial data to understand better the effect of ship motion and atmospheric flow on airwake characteristics.

Comparing data from the ST with low ship motion and cases without ship motion from the WT, the airwake response compares well between the two experiments for headwinds (and also for oblique winds, not

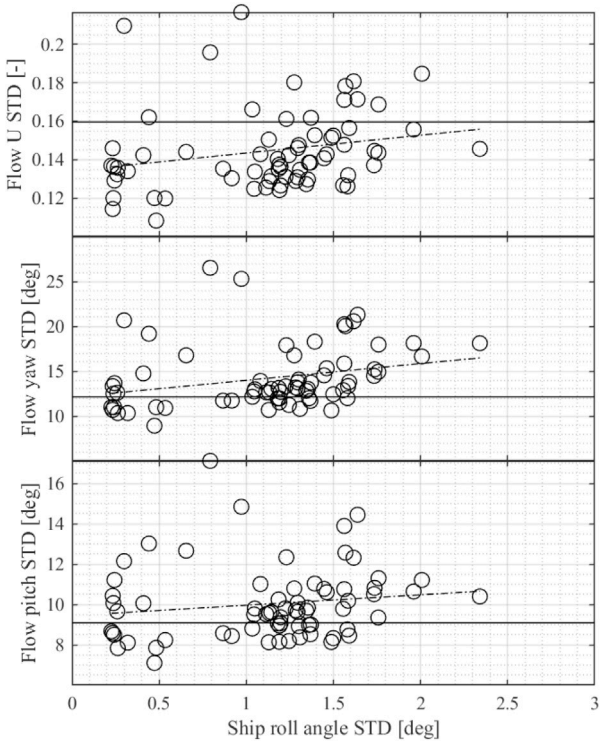

Fig. 24. Relationship between STD of ship roll and fluctuations in flow at C5.

shown). Points within the ship wake are affected by incoming flow characteristics as a secondary effect while the ship geometry dominates the flow structures.

By studying simple motions in the wind tunnel, it can be seen that ship motion adds energy to the flow at the ship motion frequency. The slower the relative wind, the more pronounced the impact. The larger the motion amplitude, the more pronounced the impact.

In general, the airwakes of ships of similar size experience a similar motion-induced characteristics. This means that motion may be less sensitive to geometric features than the static-ship component of the airwake. Larger superstructures impart a larger impact on the magnitude of the airwake response for a given motion input.

In real at-sea conditions, the combination of low frequency fluctuations in the atmosphere and ship motion conditions, overlaid on the base ship airwake in static motion conditions, define the airwake characteristics. The level of variation in the incoming wind as measured by the ship anemometers corrected for bias but not the induced-flow effects of ship motion exhibits a convincing relationship that describes the amount of extra energy added to the airwake as a result of environmental conditions.

Acronyms

ABL	atmospheric boundary layer
AOR	Auxiliary Oil Replenishment
ASL	above sea level
CFD	computational fluid dynamics
CPF	Canadian Patrol Frigate
DRDC	Defence Research and Development Canada
GD	Generic Destroyer
HH	high hover
HULMS	Helicopter Unsteady Loads Measurement System
NATO	North Atlantic Treaty Organization
NRC	National Research Council
ONR	Office of Naval Research
PIV	particle image velocimetry
SFS2	Simple Frigate Shape 2
SHOL	Ship–Helicopter Operational Limits
ST	sea trial
STD	standard deviation
WT	wind tunnel

CRediT authorship contribution statement

Alanna Wall: Conceptualization, Methodology, Validation, Formal Analysis, Writing. **Eric Thornhill:** Conceptualization, Methodology, Investigation, Writing. **Hali Barber:** Formal Analysis, Investigation, Writing. **Sean McTavish:** Conceptualization, Investigation, Review. **Richard Lee:** Conceptualization, Methodology, Investigation.

Declaration of competing interest

The authors declare that they have no known competing financial interests or personal relationships that could have appeared to influence the work reported in this paper.

References

AVT-148 Task Group, 2011. Modelling and Simulation of the Ship Environment for Safer Aircraft Launch and Recovery. NATO Research and Technology Organisation.

Bradley, R., 2004. Feasibility of Determining the Features of Ships Airwake (Ph.D. thesis). Glasgow Caledonian University.

Dooley, Gregory M., Carrica, Pablo M., Martin, J. Ezequiel, Krebill, Austin F., Buchholz, James H.J., 2019. Effects of waves, motions and atmospheric turbulence on ship airwakes. In: AIAA SciTech 2019 Forum. (AIAA 2019-1328), American Institute of Aeronautics and Astronautics, San Diego, California,

Dooley, G.M., Ezequiel, J., Buchholz, J.H.J, Carrica, P.M., 2020. Ship airwakes in waves and motions and effects on helicopter operation. Comput. Fluids 208 (104627).

Forrest, J.S., Owen, I., Padifled, G.D., Hodge, S.J., 2012. Ship-helicopter operating limits prediction using piloted flight simulation and time-accurate airwakes. J. Aircr. 49 (4).

Harrison, Sheldon, Wall, Alanna, Thornhill, Eric, 2019. Assessing pilot response to low-frequency disturbances: a literature review. In: Proceedings of the Canadian Aeronautics and Space Institute AERO 2019. Montreal, Canada.

Healey, J. Val, 1992. Establishing a database for flight in the wakes of structures. J. Aircr. 29 (4), 559–564.

Hooper, J.D., Musgrove, A.R., 1997. Reynolds stress, mean velocity, and dynamic pressure measurement by a four-hole pressure probe. Exp. Therm. Fluid Sci. 15, 375–383.

Irwin, H.P.A.H., 1979. Design and Use of Spires for Natural Wind Simulation. Technical Report LTR-LA-233, National Research Council of Canada.

Kaaria, C., Wang, T., White, M., Owen, I., 2013. An experimental technique for evaluating the aerodynamic impact of ship superstructures on helicopter operations. Ocean Eng. 61, 97–108.

Krebill, Austin, 2020. Effects of Ship Motion on Airwake Aerodynamics (Ph.D. thesis). The University of Iowa.

Lee, R.G., Zan, S.J., 2005a. Unsteady aerodynamic loads on a helicopter fuselage in a ship airwake. J. Am. Helicopter Soc. 49, 149–159.

Lee, R.G., Zan, S.J., 2005b. Wind tunnel testing of a helicopter fuselage and rotor in a ship airwake. J. Am. Helicopter Soc. 50, 326–337.

McRuer, D.T., 1994. Interdisciplinary interactions and dynamic systems integration. Int. J. Control 59 (1), 3–12.

McTaggart, K.A., 2010. Verification and validation of shipmo3d ship motion predictions in the time and frequency domains. In: International Towing Tank Conference Workshop on Seakeeping: Verification and Validation for Non-linear Seakeeping Analysis. DRDC Atlantic, Seoul, Korea.

McTavish, Sean A. M., Wall, Alanna S., Lee, Richard G., 2015. A methodology to correlate simulated airwake data and unsteady helicopter load measurements to shipboard helicopter flight test data. In: 14th International Conference on Wind Engineering.

Meroney, R.N., 1988. Wind tunnel modeling of the flow about bluff bodies. J. Wind Eng. Ind. Aerodyn. 29, 203–223.

NATO, 1993. Standardized Wave and Wind Environments and Shipboard Reporting of Sea Conditions: STANAG 4194 Ed. 2. Tech. Rep..

Owen, I., Lee, R., Wall, A., Fernandez, N., 2020. The NATO generic destroyer - A shared geometry for collaborative research into modelling and simulation of shipboard launch and recovery. Ocean Eng. 228 (108428).

Polsky, Susan, 2003. CFD prediction of airwake flowfields for ships experiencing beam winds. In: Proc. of 21st Applied Aerodynamic Conference. (AIAA 2003-3657).

Rahimpour, Mostafa, Oshkai, Peter, 2016. Experimental investigtion of airflow over the helicopter platform of a polar icebreaker. Ocean Eng. 121, 98–111.
Rhoades, M.M., Healey, J. Val., 1992. Flight deck aerodynamcis of a nonaviation ship. J. Aircr. 29 (4), 619–626.
Seth, D., Leishman, J.G., Gnanamanickam, E., Zhang, Z., 2020. Time-resolved PIV measurements of a ship airwake in simulated atmospheric boundary layer. In: AIAA Aviation 2020 Forum.
SethuRaman, S., 1979. Stucture of turbulence over water during high winds. J. Appl. Meteorol. 18 (2), 324–328.
Shi, Yongjie, He, Xiang, Xu, Yi, Xu, Guohua, 2019. Numerical study on flow control of ship airwake and rotor airload during helicopter shipboard landing. Chin. J. Aeronaut. 32 (2), 324–336.
Shipman, J.D., Arunajatesan, S., Cavallo, P.A., Sinha, N., Polsky, S.A., 2008. Dynamic CFD simulation of aircraft recovery to an aircraft carrier. In: 26th AIAA Applied Aerodynamics Conference, Vol. AIAA Paper 2008-6227. Honolulu, HI, USA.
Shukla, S., Sinha, S.S., Singh, S.N., 2019. Ship-helo coupled airwake aerodynamics: A comprehensive review. Prog. Aerosp. Sci. 106, 71–107.
Skies Magazine, 2019. Cyclone experiences hard landing. https://www.skiesmag.com/news/cyclone-experiences-hard-landing/.
Society of Rock, 2020. Crazy helicopter landing on ship during raging sea. https://societyofrock.com/crazy-helicopter-landing-on-ship-during-raging-sea/.
Sydney, Anish J., Ramsey, Joseph P., Milluzzo, Joseph I., 2017. Time-resolved PIV measurements of ship motion and orientation effects on airwake development. In: 35th AIAA Applied Aerodynamics Conference.
Thedin, R., Kinzel, M.P., Horn, J.F., Schmitz, S., 2019. Coupled simulations of atmospheric turbulence-modified ship airwakes and helicopter flight dynamics. J. Aircr. 56 (2), 812–824.
Thornhill, E., Wall, A.S., McTavish, S., Lee, R.G., 2020. Ship anemometer bias management. Ocean Eng. 216 (107843).
Wall, Alanna, Lee, Richard, Barber, Hali, 2020a. Analysis of fast-response cobra probe data in highly turbulent wake flows. https://nrc-publications.canada.ca/eng/view/object/?id=9147610b-dbe9-443b-b77a-cbb15eb3a28e.
Wall, A., Lee, R., Barber, H., Thornhill, E., 2020b. The nato generic destroyer - a shared geometry for collaborative research into modelling and simulation of shipboard launch and recovery: source data posting on open science canada. https://open.canada.ca/data/en/dataset/2c30e366-ef2b-400e-8363-0b13e4a7b6f4.
Yuan, W., Wall, A., Lee, R., 2018. Combined numerical and experimental simulations of unsteady ship airwakes. Comput. Fluids 172, 29–53.
Zan, S.J., 2001. Surface flow topology for a simple frigate shape. Can. Aeronaut. Space J. 47, 33–43.